Macromolecules

pubs.acs.org/Macromolecules Article

Strong Variation of Micelle–Unimer Coexistence as a Function of Core Chain Mobility

Ryan J. Carrazzone,[‡] Xiuli Li,[‡] Jeffrey C. Foster, Veera Venkata Shravan Uppala, Candace E. Wall, Alan R. Esker, Louis A. Madsen,* and John B. Matson*

Cite This: *Macromolecules* 2021, 54, 6975–6981 Read Online

ACCESS | Metrics & More | Article Recommendations | Supporting Information

ABSTRACT: Polymeric micelles coexist in solution with unassembled chains (unimers). We have investigated the influence of glass transition temperature (T_g) (i.e., chain mobility) of the micelle core-forming blocks on micelle–unimer coexistence. We synthesized a series of seven PEG-*b*-P(*n*BA-*ran*-*t*BA) amphiphilic block copolymers [PEG = poly(ethylene glycol), *n*BA = *n*-butyl acrylate, and *t*BA = *tert*-butyl acrylate] with similar molecular weights (12 kg/mol). Varying the *n*BA/*t*BA molar ratio enabled the broad modulation of core block T_g with no significant change in core hydrophobicity or micelle size. NMR diffusometry revealed increasing unimer populations from 0 to 54% of total polymer concentration upon decreasing core block T_g from 25 to −46 °C. Additionally, unimer population at fixed polymer composition (and thus core T_g) increased with temperature. This study demonstrates the strong influence of core-forming block mobility on polymer self-assembly, providing information toward designing drug delivery systems and suggesting the need for a new dynamical theory.

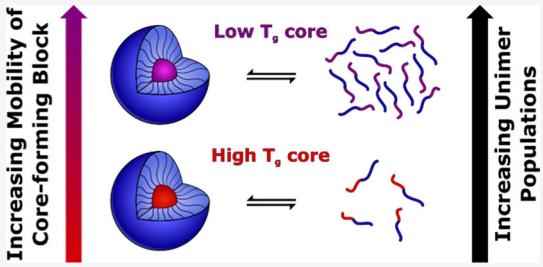

INTRODUCTION

The spontaneous association of molecules by noncovalent interactions to form higher order structures, termed molecular self-assembly or simply self-assembly,[1] is pervasive throughout nature, often originating from regions of differing hydrophobicity among associating molecules. For example, key cellular components derive their structure and function largely from self-assembly, including cell membranes,[2] actin fibers,[3] and vesicles.[4] Synthetic materials, notably amphiphilic block copolymers (BCPs), also self-assemble to generate nanoscopic hydrophobic/hydrophilic domains that enable various applications ranging from delivery vehicles for hydrophobic drugs[5−9] to scaffolds for the synthesis of unique polymer architectures[10−12] and to nanoscale compartments for catalysis.[13,14] As a result, a fundamental understanding of the parameters governing the self-assembly of small molecules[15−17] and BCPs[18,19] has been established.

Amphiphilic BCPs exhibit various morphologies in bulk[20,21] and in solution,[22,23] and polymer characteristics [e.g., hydrophobicity of the core-forming block, ratio of hydrophilic to hydrophobic content, and glass transition temperature (T_g) of the core-forming block] can greatly influence their self-assembly.[24−27] Beyond polymer characteristics, the solution composition and preparation technique can also dramatically impact self-assembly.[19,28−30] However, despite the vast amount of research investigating the morphologies and self-assembly processes of amphiphilic BCPs, there is limited information on the equilibrium between nanostructures and free polymer chains in solution (unimers). This gap in the field is due in part to the typically low concentration of unimers relative to associated polymer chains in amphiphilic BCP systems; the unimer concentration is usually assumed to be equal to the critical micelle concentration,[31] which is generally below the detection limit of common characterization techniques.[32−34] Furthermore, unimer populations can significantly impact the pharmacokinetics and biodistribution of amphiphilic BCPs.[35−37] As a result, there is growing interest in developing techniques to reliably quantify unimer populations.

One technique well suited for quantifying unimer populations in micelles is pulsed-field-gradient NMR diffusometry. This NMR technique is nondestructive and enables sensitive determination of diffusion coefficients for various mobile species in solution and in solid materials. Furthermore, NMR diffusometry can track species with molecular and elemental specificity, and thus, it has been used to observe multiple diffusing species in a wide range of polymeric systems.[38−44] Relevant to this work, NMR diffusometry experiments can measure unimer and micelle populations for BCP systems.[33,34]

In this work, we aimed to investigate the influence of core block mobility (and thus T_g) on the micelle–unimer

Received: March 21, 2021
Revised: June 14, 2021
Published: July 2, 2021

https://doi.org/10.1021/acs.macromol.1c00635
Macromolecules 2021, 54, 6975–6981

equilibrium by synthesizing a series of BCPs containing hydrophobic blocks of similar hydrophobicity but varying chain flexibility. This series of BCPs could then be analyzed by NMR diffusometry to observe the change in unimer populations as a function of two key thermodynamic variables—hydrophobic block composition and temperature. Ultimately, we envisioned that this systematic study of unimer−micelle coexistence would reveal how core block mobility affects unimer populations, which could provide information on polymer micelle designs for a variety of applications.

RESULTS AND DISCUSSION

BCP Synthesis and Characterization. Micelle core characteristics strongly impact the overall properties of a self-assembled structure, including effects such as influencing drug loading,[45] enabling fluorescent response,[46] and controlling the release of active pharmaceutical ingredients.[47] Based on these findings, we hypothesized that a relationship between the T_g of the hydrophobic, core-forming block and micelle−unimer coexistence might exist. To test this hypothesis, we needed to prepare a series of BCPs with identical hydrophilic blocks but with hydrophobic blocks that had varying T_g's but were otherwise similar in terms of molecular weight and hydrophobicity. To achieve this goal, we turned to copolymerization, a technique that has long been recognized as an effective method for modifying the T_g of polymers.[48,49] We expected that copolymerizing two monomers with similar hydrophobicity but with greatly different polymer T_g's would allow for fine-tuning of the core-forming block T_g. Two acrylate monomers, *n*-butyl acrylate (*n*BA) and *tert*-butyl acrylate (*t*BA), have similar partition coefficients (an indicator of hydrophobicity) but T_g's of −50 and 50 °C, respectively.[50,51] The isomeric *n*BA and *t*BA monomers also have reactivity ratios near 1.00 in radical copolymerization, enabling ideal random copolymerization behavior.[52] Therefore, we synthesized a series of BCPs containing poly(ethylene glycol) hydrophilic blocks and random copolymers of poly(*n*BA) and poly(*t*BA) as the hydrophobic blocks (Scheme 1).

Scheme 1. Preparation of PEG-*b*-P(*n*BA-*ran*-*t*BA) BCPs

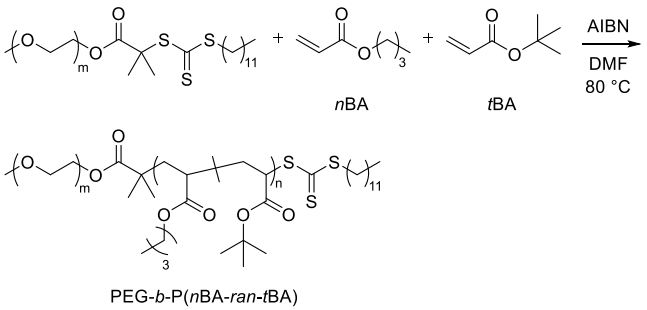

We prepared this series of BCPs with varying core block compositions in two steps. First, we synthesized a large batch of trithiocarbonate-terminated PEG to serve as the hydrophilic block in each of the BCPs (PEG M_n = 4 kg/mol). The trithiocarbonate unit served as a chain transfer agent (CTA) for reversible addition−fragmentation chain-transfer (RAFT) polymerization to control molecular weight. In the second step, we synthesized seven BCPs with varying *n*BA/*t*BA molar ratios by RAFT polymerization from the PEG CTA, yielding BCPs **1a**−**g**. By monitoring monomer disappearance over time, we found that *n*BA and *t*BA were consumed at the same rate (Figure S25), confirming that the feed ratio and composition ratio were identical. We kept the hydrophilic/hydrophobic ratio constant while systematically changing the *n*BA/*t*BA molar ratio, resulting in a series of BCPs with consistent M_n values near 12 kg/mol (Table 1).

We then evaluated each BCP by differential scanning calorimetry (DSC) to measure T_g's of the hydrophobic blocks in the bulk (Figures S26−S33). We chose to measure T_g's of the BCPs rather than P*n*BA/P*t*BA homopolymers as we expected the PEG block to influence chain mobility. As shown in Table 1 and Figure 1, the T_g's for the hydrophobic blocks of polymers **1a** (100% *n*BA) and **1g** (100% *t*BA) were −46 and 25 °C, respectively. The 100% *t*BA BCP (polymer **1g**) showed a lower T_g than the reported value of 50 °C.[51] We attribute this discrepancy to the relatively low molecular weight of the P*t*BA block and the PEG tethered to one chain end, both of which may reduce T_g. The T_g values of the hydrophobic block for BCPs **1b**−**1f** (75−25% *n*BA) closely fit approximations based on the Fox equation.[48]

Having established that the copolymerization of *n*BA and *t*BA could lead to polymers with predictable T_g values, we next aimed to confirm that copolymerization did not change the core-forming block hydrophobicity. We evaluated hydrophobicity through contact angle measurements of representative polymer films of P(*n*BA-*ran*-*t*BA) random copolymers that lacked the hydrophilic PEG block.

First, we synthesized random copolymers of *n*BA and *t*BA using RAFT with a trithiocarbonate CTA (Figures S11−S13). We chose *n*BA/*t*BA molar ratios of 1:0, 1:1, and 0:1 (polymers **2a**, **2b**, and **2c**, respectively) to span the entire series. We then prepared uniform films of polymers **2a**−**c** by spin coating from $CHCl_3$, followed by overnight drying to remove the solvent. The initial contact angle of water changed from 95° for polymer **2a** (Figure 2A) to 100° for polymer **2b** (Figure 2B) and to 95° for polymer **2c** (Figure 2C). Given the typical error in contact angle measurements of a few degrees, we conclude that the hydrophobicity remains constant across the series with varying *n*BA/*t*BA molar ratios. We also evaluated the hydrophobicity of polymers **2a** and **2c** through NMR solubility experiments. We found that P*n*BA was more soluble than P*t*BA in D_2O by a factor of 2.5, but both polymers exhibited extremely hydrophobic character (Figures S34 and S35). The solubility of PEG in water at room temperature is around 60 wt %,[53] which is a factor of ∼10^3 larger than the solubility of either acrylate polymer. As the solubility of the BCPs in water is governed primarily by the hydrophilic PEG block, we do not expect this small change in solubility to account for any differences in unimer percentages. Thus, we conclude that the hydrophobicity of the core-forming block for polymers **1a**−**g** does not change across the series.

Micelle Preparation and Characterization. After determining that T_g varies with the *n*BA/*t*BA molar ratio for polymers **1a**−**g** and that the hydrophobicity of the core-forming block does not change significantly, we next sought to investigate the change in micelle−unimer coexistence across the series. To prepare micelles from each amphiphilic BCP, we used the solvent switch method. Briefly, we first dissolved each polymer in tetrahydrofuran (THF), a good solvent for both blocks. We then diluted these polymer solutions by the dropwise addition of H_2O to generate 12.5% THF in H_2O

https://doi.org/10.1021/acs.macromol.1c00635
Macromolecules 2021, 54, 6975−6981

Table 1. Characterization of PEG-*b*-P(*n*BA-*ran*-*t*BA) BCPs

	polymer					micelle	
polymer	mol % *n*BA[a]	$M_{n\ (NMR)}$(kg/mol)[b]	$M_{n\ (SEC)}$ (kg/mol)[c]	$Đ$[c]	T_g (°C)[d]	D_h (nm)[e]	N_{agg}[f]
1a	100	12.0	12.2	1.07	−46	25.1 ± 0.1	83
1b	75	11.3	12.6	1.07	−35	28.9 ± 0.1	103
1c	60	11.9	11.9	1.12	−24	27.9 ± 0.1	101
1d	50	12.1	13.3	1.10	−20	26.2 ± 0.2	80
1e	40	11.6	11.7	1.11	−6	27.1 ± 0.6	77
1f	25	12.6	12.9	1.08	5	27.0 ± 0.2	87
1g	0	11.6	11.8	1.05	25	26.2 ± 0.5	72

[a]*n*BA/*t*BA molar ratio measured by ^{1}H NMR spectroscopy. [b]Measured by end-group analysis via ^{1}H NMR spectroscopy (Figures S14−S20). [c]Measured by size exclusion chromatography (SEC) in THF at 30 °C with multiangle light scattering (Figures S4−S10). [d]Of the hydrophobic block measured by DSC with a modulated heating rate (3 °C/min, ±2.5 °C, 60 s); data reported from the second heat cycle (Figures S26−S33). [e]Intensity average hydrodynamic diameter measured by DLS at 5 mg/mL in DI H_2O at rt (Figure S36). [f]Aggregation number derived by dividing M_w of micelle by M_w of BCP; M_w of micelles determined by SLS at 5 mg/mL in DI H_2O at rt (Figure S37 and eq S1).

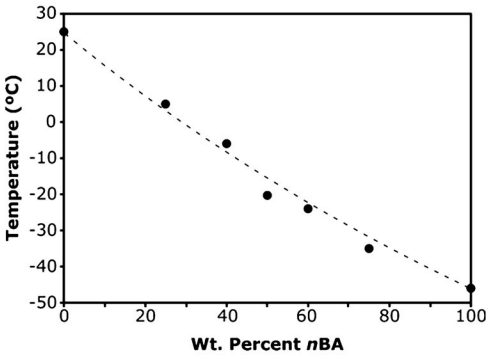

Figure 1. T_g for core-forming blocks of polymers **1a−g** (black circles) vs wt % *n*BA in the BCPs measured by DSC with a modulated heating rate (3 °C/min, ±2.5 °C, 60 s). The dotted black line represents a fit using the Fox equation (eq S2) to the measured homopolymer T_g's. The core-forming block T_g varies predictably with polymer composition, providing access to a wide range of micelle core mobilities.

solutions. We subsequently transferred the polymer solutions to dialysis tubing (MWCO 8 kDa) and dialyzed against H_2O.

We utilized dynamic light scattering (DLS) to analyze the micelle size distributions from each BCP formulation (Tables 1 and S1 and Figure S36). We observed intensity-average hydrodynamic diameters ranging from 25.1 to 28.9 nm, with no apparent trend in micelle size relating to micelle core mobility. This narrow size range is expected due to the similar molecular weights and hydrophobic weight fractions of the BCPs. Additionally, we observed low micelle polydispersity indices for each sample, indicating that samples were free of high-molecular-weight aggregates. We then employed static light scattering (SLS) to obtain the M_w of micelles in solution for each micelle sample (Figure S37). From the SLS data, we estimated the aggregation number (N_{agg}) of each sample by dividing micelle M_w by the M_w of each respective BCP (Table 1 and eq S1). We observed N_{agg} values ranging from 72 to 103, again with no apparent relation to micelle core mobility, reinforcing that the *n*BA/*t*BA molar ratio in the core-forming block did not influence polymer micelle size.

NMR Diffusometry Studies. Despite similar micelle sizes, we expected the varying chain mobility of core-forming blocks throughout polymers **1a−g** to yield differences in micelle−unimer coexistence. We first investigated the mobility of the hydrophobic core blocks with one-dimensional (1D) ^{1}H NMR spectroscopy. In the NMR spectra of polymer solutions with relatively slow chain dynamics (where spectrometer shims do not determine linewidth), the full width at half-maximum (fwhm) of peaks is inversely proportional to the spin−spin relaxation time (T_2) via the relation fwhm = $1/\pi T_2$. T_2 characterizes the dephasing of net magnetization in the transverse plane and provides information on molecular mobility.[33,54] In other words, decreasing T_2 values result in broader signal linewidths, which indicate molecular environments with increasingly limited mobility. As shown in Figure 3A, *n*BA and *t*BA alkyl proton peaks appear in the range of 0.5−2 ppm in the spectra for BCPs **1a**, **1d**, and **1g**. For 100% *n*BA polymer micelles (polymer **1a**, shown in purple), the alkyl proton peak(s) fwhm is ≈40 Hz compared to ≈80 Hz for 50% *n*BA polymer micelles (polymer **1d**, shown in green) and ≈200

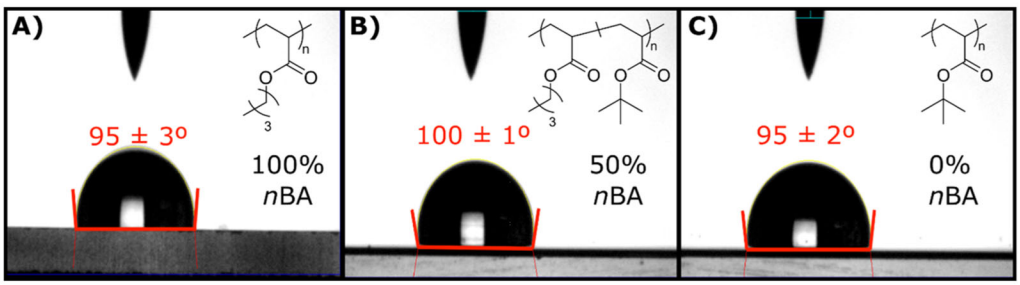

Figure 2. Initial contact angle measurements of water droplets on films of polymers **2a−c**. Polymer films were created by spin-coating polymer solutions (5 wt % in $CHCl_3$) at 5000 rpm onto glass slides, followed by drying at 30 °C. Contact angle measurements were performed in triplicate with representative images and average results reported. The relatively consistent contact angle implies that the degree of hydrophobicity (intermolecular interactions) does not depend on the *n*BA/*t*BA molar ratio.

https://doi.org/10.1021/acs.macromol.1c00635
Macromolecules 2021, 54, 6975−6981

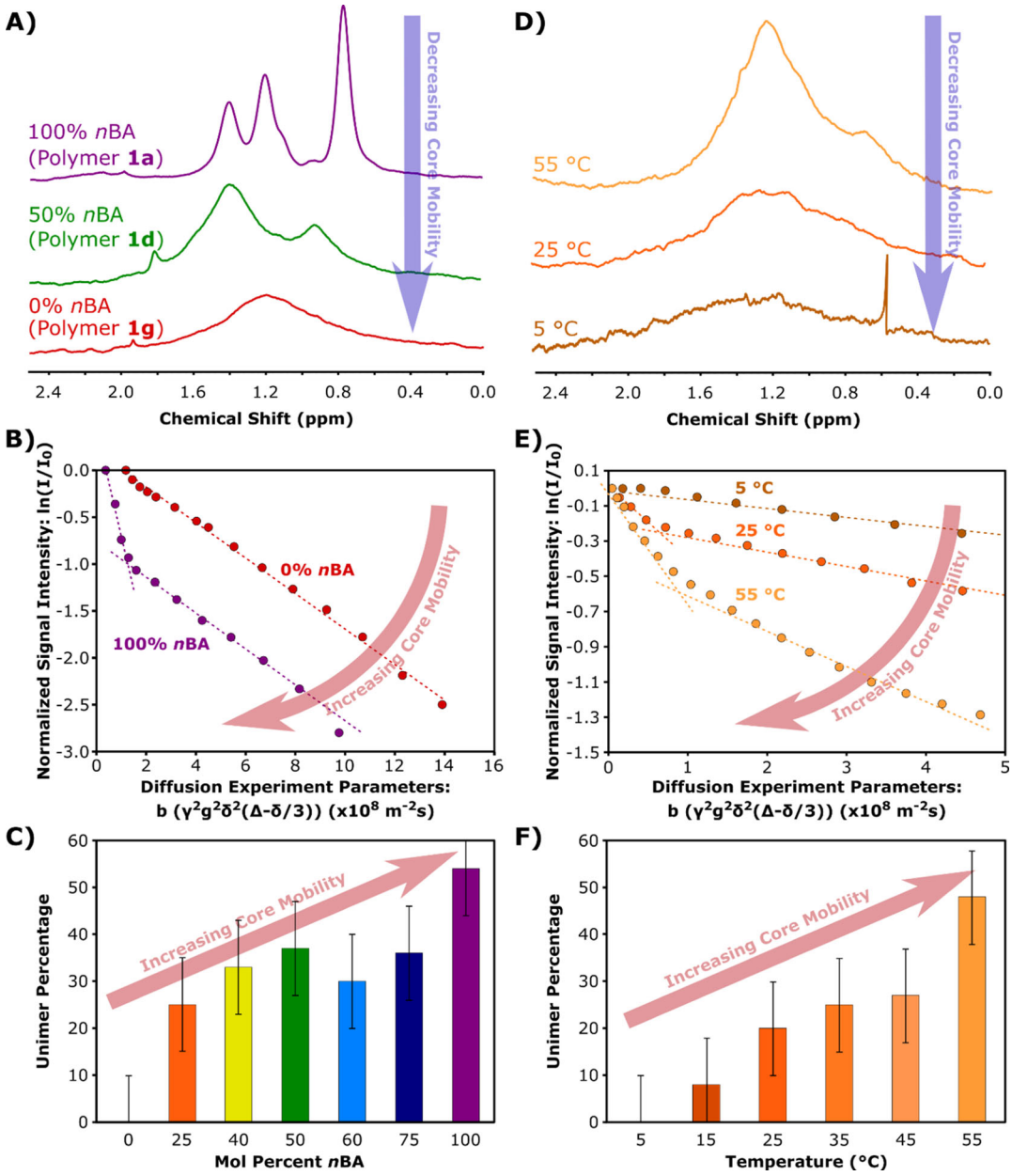

Figure 3. (A) 1D ^{1}H NMR spectra overlay of micelle solutions made from 100, 50, and 0 mol % *n*BA BCPs (polymers **1a**, **1d**, and **1g**, respectively) at 5 mg/mL in the H_2O solvent. (B) Stejskal−Tanner plots of micelle solutions as a function of core-forming block composition at 25 °C (*b* is the Stejskal−Tanner factor, *g* is the magnetic gradient strength, γ is the gyromagnetic ratio of the nucleus probed, δ is the gradient pulse duration, and Δ is the gradient pulse spacing). Dashed lines are included as a guide to the eye and represent single- or two-component diffusion coefficients (they do not represent fit lines). (C) Unimer percentages derived from signal decay curves for micelle solutions as a function of core-forming block composition. (D) 1D ^{1}H NMR spectra overlay of 25% *n*BA polymer micelle solutions (from polymer **1f**) at 5, 25, and 55 °C at 5 mg/mL (see also Figure S50 for similar plots for 0% and 50% *n*BA polymers). (E) Stejskal−Tanner plots of polymer **1f** micelle solutions as a function of temperature with dashed lines as a guide to the eye for single- or two-component diffusion coefficients (they do not represent fit lines). (F) Unimer percentages derived from signal decay curves for polymer **1f** micelle solutions as a function of temperature. Strikingly, core mobility strongly correlates with micelle−unimer coexistence. Error bars are ±10% for unimer percentages.

Hz for 0% *n*BA polymer micelles (polymer **1g**, shown in red). The broadening of alkyl region signals with increasing *t*BA content in the core block signifies reduced chain mobility in the micelle cores. This result agrees with the trend of increasing measured T_g for core blocks with increasing *t*BA content.

To further investigate the influence of core-forming block T_g on micelle dynamics and on populations of unimers and micelles in solution, we then employed NMR diffusometry to probe translational motion of the different mobile populations. In brief, NMR diffusometry involves the principle that if there are chemical species of differing mobility that do not exchange quickly relative to the time scale of diffusion (Δ = 25 ms in this study, see the Supporting Information for details), we can extract distinct diffusion coefficients for each moving species. In amphiphilic BCP systems, diffusion rates of unassembled unimeric polymer chains versus assembled nanostructures (micelles) in solution are sufficiently different such that we can also extract the relative populations of each species.[33,34] We access the relative populations of unimers versus micelle

https://doi.org/10.1021/acs.macromol.1c00635
Macromolecules 2021, 54, 6975−6981

assemblies through Stejskal−Tanner signal attenuation plots. By plotting the natural log of normalized NMR signal intensity (I/I_0) versus the b factor that contains all known NMR experimental parameters [$\gamma^2\delta^2g^2(\Delta - \delta/3)$, see the Supporting Information for details] in a signal attenuation curve, we extract diffusion coefficients D from linear regressions. A single linear fit indicates a single diffusing species in solution, while multicomponent fitting implies multiple species diffusing at different rates. In a micellar system, fast-diffusing unimers contribute to a rapid signal decay at lower magnetic gradient strength (g), while slower-diffusing micelles contribute to a slow signal decay at higher gradient strength. As such, the signal decay curve of a sample containing both micelles and unimers shows rapid decay at low gradient strength, followed by more gradual decay at higher gradient strengths. The relative intensities (weighting) of these decay regimes can then yield the micelle and unimer populations in the sample.

Throughout this BCP series, we observed significant changes in the signal decay curves, demonstrating shifts in the micelle−unimer equilibrium. As shown in Figure 3B, 100% *n*BA polymer micelles (polymer **1a**, shown in purple) and 0% *n*BA polymer micelles (polymer **1g**, shown in red) displayed drastically different signal decay curves. The 0% *n*BA polymer micelles showed a relatively slow signal decay curve with a single-component linear fit, which corresponds to a single diffusing species in solution (micelles). Conversely, the 100% *n*BA polymer micelles exhibited a signal decay curve with a two-component fit, indicating that there were two diffusing species in solution (slow-diffusing micelles and fast-diffusing unimers). As previously mentioned, the experimental timescale is much faster than unimer exchange, signifying that these differences in micelle−unimer coexistence do not arise from differences in unimer exchange kinetics. We have measured free unimer content on heating and cooling on other BCP micelles and have so far obtained the same free versus micelle-associated unimer fractions.[34]

To evaluate the influence of core block T_g on micelle−unimer coexistence, we extracted the micelle and unimer populations for the solutions of polymers **1a−g** from fits to their signal decay curves, as shown in Figure 3C (also Figures S38−S42). The stark difference in unimer populations between the 100 and 0% *n*BA micelles suggests that the 0% *n*BA micelles exist in a "frozen core" state at the temperature of the NMR experiment (25 °C).[55] Interestingly, NMR diffusometry experiments before and after thermal annealing of several samples revealed no changes in the unimer percentage (Figures S43−S45), indicating that these results are thermally robust and reversible and are due to differences in chain mobility (or some system parameters closely correlated with mobility) and not due to the kinetic trapping of micelle chains. Additionally, NMR diffusometry experiments on 25% *n*BA micelles (polymer **1f**) at concentrations ranging from 3 to 10 mg/mL revealed no changes in unimer percentages (Figure S46). Overall, we observed a general trend of increasing unimer population with decreasing core-forming block T_g throughout the series, with three notable regimes of unimer percentages (0−10, 20−30, and 40−50), indicating a relationship between core mobility and unimer population. In traditional theories of micellization,[15,16,18,19] core molecular dynamics should not explicitly affect micelle−unimer equilibrium partitioning, but the present results suggest that a new theory may be needed.

We also performed NMR diffusometry experiments on a 25% *n*BA micelle sample (polymer **1f**, T_g = 5 °C) as a function of temperature. As shown in Figure 3D, the micelle core exhibited higher mobility (narrower signal linewidths) at elevated temperature (55 °C) and showed the lowest mobility at $T = T_g$. NMR diffusometry signal decay curves for 25% *n*BA micelles at different temperatures, as shown in Figure 3E, showed significant increases in unimer population with increasing temperature, as expected based on the results from the compositional experiments summarized in Figure 3C. Additionally, unimer populations derived from the signal decay curves, as shown in Figure 3F (also Figures S47−S49), increased with temperature and fell within the three regimes we had observed during the compositional experiments, reinforcing our hypothesis that micelle core mobility directly impacts micelle−unimer coexistence. Variable-temperature NMR diffusometry experiments on two other polymer micelle compositions (polymers **1d** and **1g**, 50 and 0% nBA, respectively) revealed a consistent population of 40−50% unimers for high core mobility micelles (polymer **1d**) and a change from 0 to 25% unimers with increasing temperature past the T_g for low core mobility micelles (polymer **1g**) (Figure S50). However, we recognize that temperature affects other aspects of the system as well, including solvent quality and interfacial tension,[56] so although the correlation is strong between core mobility and free unimer percentage, these results may not be solely due to increasing core mobility with increasing temperature.

We also note that we explored the time required to reach quasi-equilibrium conditions for these micelles. For representative compositions and temperatures (Figures S43−S50), we measured diffusion immediately after making any temperature changes in quick (5−10 min) intervals and found that the measurements (diffusion coefficient values and free unimer fractions) reached plateau values after 30 min and did not further evolve for at least a month. This demonstrates that, once formulated, these micellar systems come to quasi-equilibrium rapidly and then are stable for periods longer than that are relevant to drug delivery technologies.

The assembly of polymer amphiphiles into micelles is a thermodynamic process, driven by the increased entropy of water molecules excluded from the core and the increased hydrophobic interactions of the core-forming block.[18] Because the mobility of the core-forming block should not theoretically impact micelle−unimer coexistence and would instead be more important for kinetic processes (i.e., unimer exchange), we are working to further investigate how micelle core mobility impacts unimer populations.

■ CONCLUSIONS

In summary, we have explored in detail the relationship between micelle core mobility and micelle−unimer coexistence. By synthesizing and characterizing a series of amphiphilic BCPs with varying *n*BA/*t*BA molar ratios in the hydrophobic blocks, we observed an overall trend of increasing unimer populations with decreasing T_g of the core-forming block. We verified the decoupling of effects of core chain mobility (varying T_g and experimental temperature) from changes in micelle core hydrophobicity via contact angle measurements of homopolymer films and NMR solubility experiments on *n*BA/*t*BA homopolymers, which showed no significant difference in hydrophobicity relative to the *n*BA/*t*BA molar ratio. We investigated the relationship between core

https://doi.org/10.1021/acs.macromol.1c00635
Macromolecules 2021, 54, 6975−6981

mobility and unimer population by variable-temperature NMR spectroscopy and diffusometry experiments, which showed increasing unimer population and chain mobility with increasing temperature. Our results contradict the usual assumption from micellar theory that the chain mobility of the core should have no effect on polymer chain phase behavior (i.e., micelle−unimer coexistence), thus leading to potentially new directions in theoretical study. We expect that these findings will provide new insights into micellar behaviors and future designs for amphiphilic BCP systems, particularly in applications where large unimer concentrations may induce undesired (or desired) effects.

■ ASSOCIATED CONTENT

Supporting Information

The Supporting Information is available free of charge at https://pubs.acs.org/doi/10.1021/acs.macromol.1c00635.

Synthetic procedures, polymer and polymer aggregate characterization, NMR diffusometry experimental data, and NMR signal acquisition parameters (PDF)

■ AUTHOR INFORMATION

Corresponding Authors

Louis A. Madsen − *Department of Chemistry and Macromolecules Innovation Institute, Virginia Tech, Blacksburg, Virginia 24061, United States;* orcid.org/0000-0003-4588-5183; Email: lmadsen@vt.edu

John B. Matson − *Department of Chemistry and Macromolecules Innovation Institute, Virginia Tech, Blacksburg, Virginia 24061, United States;* orcid.org/0000-0001-7984-5396; Email: jbmatson@vt.edu

Authors

Ryan J. Carrazzone − *Department of Chemistry and Macromolecules Innovation Institute, Virginia Tech, Blacksburg, Virginia 24061, United States*

Xiuli Li − *Department of Chemistry and Macromolecules Innovation Institute, Virginia Tech, Blacksburg, Virginia 24061, United States*

Jeffrey C. Foster − *Department of Chemistry and Macromolecules Innovation Institute, Virginia Tech, Blacksburg, Virginia 24061, United States;* Present Address: Sandia National Lab, Albuquerque, NM, 87123; orcid.org/0000-0002-9097-8680

Veera Venkata Shravan Uppala − *Department of Chemistry and Macromolecules Innovation Institute, Virginia Tech, Blacksburg, Virginia 24061, United States*

Candace E. Wall − *Department of Chemistry and Macromolecules Innovation Institute, Virginia Tech, Blacksburg, Virginia 24061, United States*

Alan R. Esker − *Department of Chemistry and Macromolecules Innovation Institute, Virginia Tech, Blacksburg, Virginia 24061, United States*

Complete contact information is available at: https://pubs.acs.org/10.1021/acs.macromol.1c00635

Author Contributions

‡R.J.C. and X.L. contributed equally to this work.

Notes

The authors declare no competing financial interest.

■ ACKNOWLEDGMENTS

This work was supported by the US National Science Foundation (CBET 1437767 and CHE 1904746 and 2003662) and the US National Institutes of Health (R01GM123508). We thank Prof. Richey Davis for helpful discussions and for the use of the DLS instrument, Prof. Tim Long and Dr. Ryan Mondschein for DSC assistance, and Kearsley Dillon, Sarah Swilley-Sanchez, and Yumeng (Jackie) Zhu for critical readings of the manuscript. Any opinions, findings, and conclusions or recommendations expressed in this material are those of the authors and do not necessarily reflect the views of the funding agencies.

■ REFERENCES

(1) Jones, R. G.; Ober, C. K.; Hodge, P.; Kratochvíl, P.; Moad, G.; Vert, M. Terminology for aggregation and self-assembly in polymer science (IUPAC Recommendations 2013). *Pure Appl. Chem.* **2012**, *85*, 463−492.

(2) Bangham, A. D. Liposomes: The Babraham connection. *Chem. Phys. Lipids* **1993**, *64*, 275−285.

(3) Dobson, C. M. Protein folding and misfolding. *Nature* **2003**, *426*, 884−890.

(4) Discher, D. E.; Eisenberg, A. Polymer Vesicles. *Science* **2002**, *297*, 967.

(5) Allen, T. M.; Cullis, P. R. Liposomal drug delivery systems: From concept to clinical applications. *Adv. Drug Delivery Rev.* **2013**, *65*, 36−48.

(6) Allen, T. M.; Cullis, P. R. Drug Delivery Systems: Entering the Mainstream. *Science* **2004**, *303*, 1818.

(7) Adams, M. L.; Lavasanifar, A.; Kwon, G. S. Amphiphilic block copolymers for drug delivery. *J. Pharm. Sci.* **2003**, *92*, 1343−1355.

(8) Biswas, S.; Kumari, P.; Lakhani, P. M.; Ghosh, B. Recent advances in polymeric micelles for anti-cancer drug delivery. *Eur. J. Pharm. Sci.* **2016**, *83*, 184−202.

(9) Kataoka, K.; Harada, A.; Nagasaki, Y. Block copolymer micelles for drug delivery: Design, characterization and biological significance. *Adv. Drug Delivery Rev.* **2012**, *64*, 37−48.

(10) Cheng, C.; Qi, K.; Khoshdel, E.; Wooley, K. L. Tandem Synthesis of Core−Shell Brush Copolymers and Their Transformation to Peripherally Cross-Linked and Hollowed Nanostructures. *J. Am. Chem. Soc.* **2006**, *128*, 6808−6809.

(11) Ievins, A. D.; Moughton, A. O.; O'Reilly, R. K. Synthesis of Hollow Responsive Functional Nanocages Using a Metal−Ligand Complexation Strategy. *Macromolecules* **2008**, *41*, 3571−3578.

(12) Moughton, A. O.; O'Reilly, R. K. Noncovalently Connected Micelles, Nanoparticles, and Metal-Functionalized Nanocages Using Supramolecular Self-Assembly. *J. Am. Chem. Soc.* **2008**, *130*, 8714−8725.

(13) Gallou, F.; Isley, N. A.; Ganic, A.; Onken, U.; Parmentier, M. Surfactant technology applied toward an active pharmaceutical ingredient: More than a simple green chemistry advance. *Green Chem.* **2016**, *18*, 14−19.

(14) Klingelhöfer, S.; Heitz, W.; Greiner, A.; Oestreich, S.; Förster, S.; Antonietti, M. Preparation of Palladium Colloids in Block Copolymer Micelles and Their Use for the Catalysis of the Heck Reaction. *J. Am. Chem. Soc.* **1997**, *119*, 10116−10120.

(15) Israelachvili, J. N.; Mitchell, D. J.; Ninham, B. W. Theory of self-assembly of hydrocarbon amphiphiles into micelles and bilayers. *J. Chem. Soc., Faraday Trans.* **1976**, *72*, 1525−1568.

(16) Israelachvili, J. N.; Marčelja, S.; Horn, R. G. Physical principles of membrane organization. *Q. Rev. Biophys.* **1980**, *13*, 121−200.

(17) Fong, C.; Le, T.; Drummond, C. J. Lyotropic liquid crystal engineering−ordered nanostructured small molecule amphiphile self-assembly materials by design. *Chem. Soc. Rev.* **2012**, *41*, 1297−1322.

(18) Mai, Y.; Eisenberg, A. Self-assembly of block copolymers. *Chem. Soc. Rev.* **2012**, *41*, 5969−5985.

(19) Riess, G. Micellization of block copolymers. *Prog. Polym. Sci.* **2003**, *28*, 1107−1170.
(20) Darling, S. B. Directing the self-assembly of block copolymers. *Prog. Polym. Sci.* **2007**, *32*, 1152−1204.
(21) Bates, F. S.; Fredrickson, G. Block copolymers—designer soft materials. *Phys. Today* **2000**, *52*, 32.
(22) Williams, R. J.; Pitto-barry, A.; Kirby, N.; Dove, A. P.; Reilly, R. K. O. Cyclic Graft Copolymer Unimolecular Micelles: Effects of Cyclization on Particle Morphology and Thermoresponsive Behavior. *Macromolecules* **2016**, *49*, 2802.
(23) Zhang, L.; Eisenberg, A. Multiple Morphologies and Characteristics of "Crew-Cut" Micelle-like Aggregates of Polystyrene-*b*-poly(acrylic acid) Diblock Copolymers in Aqueous Solutions. *J. Am. Chem. Soc.* **1996**, *118*, 3168−3181.
(24) Shen, H.; Eisenberg, A. Block Length Dependence of Morphological Phase Diagrams of the Ternary System of PS-*b*-PAA/Dioxane/H_2O. *Macromolecules* **2000**, *33*, 2561−2572.
(25) Figg, C. A.; Carmean, R. N.; Bentz, K. C.; Mukherjee, S.; Savin, D. A.; Sumerlin, B. S. Tuning Hydrophobicity To Program Block Copolymer Assemblies from the Inside Out. *Macromolecules* **2017**, *50*, 935−943.
(26) Yamamoto, Y.; Yasugi, K.; Harada, A.; Nagasaki, Y.; Kataoka, K. Temperature-related change in the properties relevant to drug delivery of poly (ethylene glycol)−poly (D,L-lactide) block copolymer micelles in aqueous milieu. *J. Controlled Release* **2002**, *82*, 359−371.
(27) Foster, J. C.; Varlas, S.; Couturaud, B.; Jones, J. R.; Keogh, R.; Mathers, R. T.; O'Reilly, R. K. Predicting Monomers for Use in Polymerization-Induced Self-Assembly. *Angew. Chem., Int. Ed.* **2018**, *57*, 15733−15737.
(28) Choucair, A.; Eisenberg, A. Control of amphiphilic block copolymer morphologies using solution conditions. *Eur. Phys. J. E* **2003**, *10*, 37−44.
(29) Zhang, L.; Eisenberg, A. Thermodynamic vs Kinetic Aspects in the Formation and Morphological Transitions of Crew-Cut Aggregates Produced by Self-Assembly of Polystyrene-*b*-poly(acrylic acid) Block Copolymers in Dilute Solution. *Macromolecules* **1999**, *32*, 2239−2249.
(30) Cui, H.; Chen, Z.; Zhong, S.; Wooley, K. L.; Pochan, D. J. Block Copolymer Assembly via Kinetic Control. *Science* **2007**, *317*, 647.
(31) Oerlemans, C.; Bult, W.; Bos, M.; Storm, G.; Nijsen, J. F. W.; Hennink, W. E. Polymeric Micelles in Anticancer Therapy: Targeting, Imaging and Triggered Release. *Pharm. Res.* **2010**, *27*, 2569−2589.
(32) Nakamura, K.; Endo, R.; Takeda, M. Surface properties of styrene−ethylene oxide block copolymers. *J. Polym. Sci., Polym. Phys. Ed.* **1976**, *14*, 1287−1295.
(33) Kidd, B. E.; Li, X.; Piemonte, R. C.; Cooksey, T. J.; Singh, A.; Robertson, M. L.; Madsen, L. A. Tuning Biocompatible Block Copolymer Micelles by Varying Solvent Composition: Dynamics and Populations of Micelles and Unimers. *Macromolecules* **2017**, *50*, 4335−4343.
(34) Li, X.; Cooksey, T. J.; Kidd, B. E.; Robertson, M. L.; Madsen, L. A. Mapping Coexistence Phase Diagrams of Block Copolymer Micelles and Free Unimer Chains. *Macromolecules* **2018**, *51*, 8127−8135.
(35) Batrakova, E.; Lee, S.; Li, S.; Venne, A.; Alakhov, V.; Kabanov, A. Fundamental Relationships Between the Composition of Pluronic Block Copolymers and Their Hypersensitization Effect in MDR Cancer Cells. *Pharm. Res.* **1999**, *16*, 1373−1379.
(36) Batrakova, E. V.; Li, S.; Li, Y.; Alakhov, V. Y.; Elmquist, W. F.; Kabanov, A. V. Distribution kinetics of a micelle-forming block copolymer Pluronic P85. *J. Controlled Release* **2004**, *100*, 389−397.
(37) Panova, I. G.; Spiridonov, V. V.; Kaplan, I. B.; Trubinov, S. S.; Elizova, N. V.; Melnichenko, A. A.; Orekhov, A. N.; Yaroslavov, A. A. Inhibitory effect of polyethylene oxide and polypropylene oxide triblock copolymers on aggregation and fusion of atherogenic low density lipoproteins. *Biochemistry (Moscow)* **2015**, *80*, 1057−1064.
(38) Pettersson, E.; Topgaard, D.; Stilbs, P.; Söderman, O. Surfactant/Nonionic Polymer Interaction. A NMR Diffusometry and NMR Electrophoretic Investigation. *Langmuir* **2004**, *20*, 1138−1143.
(39) Frise, A. E.; Pagès, G.; Shtein, M.; Pri Bar, I.; Regev, O.; Furó, I. Polymer Binding to Carbon Nanotubes in Aqueous Dispersions: Residence Time on the Nanotube Surface As Obtained by NMR Diffusometry. *J. Phys. Chem. B* **2012**, *116*, 2635−2642.
(40) Ulrich, K.; Galvosas, P.; Kärger, J.; Grinberg, F. Effects of Self-Assembly on Diffusion Mechanisms of Triblock Copolymers in Aqueous Solution. *Phys. Rev. Lett.* **2009**, *102*, 037801.
(41) Thieu, L. M.; Zhu, L.; Korovich, A. G.; Hickner, M. A.; Madsen, L. A. Multiscale Tortuous Diffusion in Anion and Cation Exchange Membranes. *Macromolecules* **2019**, *52*, 24−35.
(42) Wilmsmeyer, K. G.; Li, X.; Madsen, L. A. Anisotropic viscoelasticity and molecular diffusion in nematic wormlike micelles. *Liq. Cryst.* **2018**, *45*, 844−856.
(43) Kidd, B. E.; Forbey, S. J.; Steuber, F. W.; Moore, R. B.; Madsen, L. A. Multiscale Lithium and Counterion Transport in an Electrospun Polymer-Gel Electrolyte. *Macromolecules* **2015**, *48*, 4481−4490.
(44) Bostwick, J. E.; Zanelotti, C. J.; Iacob, C.; Korovich, A. G.; Madsen, L. A.; Colby, R. H. Ion Transport and Mechanical Properties of Non-Crystallizable Molecular Ionic Composite Electrolytes. *Macromolecules* **2020**, *53*, 1405−1414.
(45) Yamamoto, T.; Yokoyama, M.; Opanasopit, P.; Hayama, A.; Kawano, K.; Maitani, Y. What are determining factors for stable drug incorporation into polymeric micelle carriers? Consideration on physical and chemical characters of the micelle inner core. *J. Controlled Release* **2007**, *123*, 11−18.
(46) Yan, Q.; Yuan, J.; Yuan, W.; Zhou, M.; Yin, Y.; Pan, C. Copolymer logical switches adjusted through core-shell micelles: From temperature response to fluorescence response. *Chem. Commun.* **2008**, *46*, 6188−6190.
(47) Foster, J. C.; Carrazzone, R. J.; Spear, N. J.; Radzinski, S. C.; Arrington, K. J.; Matson, J. B. Tuning H_2S Release by Controlling Mobility in a Micelle Core. *Macromolecules* **2019**, *52*, 1104−1111.
(48) Fox, T. Influence of Diluent and Copolymer Composition on the Glass Temperature of a Polymer System. *Bull. Am. Phys. Soc.* **1956**, *1*, 123.
(49) Saby-Dubreuil, A.-C.; Guerrier, B.; Allain, C.; Johannsmann, D. Glass transition induced by solvent desorption for statistical MMA/nBMA copolymers — Influence of copolymer composition. *Polymer* **2001**, *42*, 1383−1391.
(50) Yamauchi, K.; Lizotte, J. R.; Long, T. E. Thermoreversible Poly(alkyl acrylates) Consisting of Self-Complementary Multiple Hydrogen Bonding. *Macromolecules* **2003**, *36*, 1083−1088.
(51) Tsui, O. K. C.; Wang, X. P.; Ho, J. Y. L.; Ng, T. K.; Xiao, X. Studying Surface Glass-to-Rubber Transition Using Atomic Force Microscopic Adhesion Measurements. *Macromolecules* **2000**, *33*, 4198−4204.
(52) Min, K.; Kwon Oh, J.; Matyjaszewski, K. Preparation of gradient copolymers via ATRP in miniemulsion. II. Forced gradient. *J. Polym. Sci., Part A: Polym. Chem.* **2007**, *45*, 1413−1423.
(53) Chen, J.; Spear, S. K.; Huddleston, J. G.; Rogers, R. D. Polyethylene glycol and solutions of polyethylene glycol as green reaction media. *Green Chem.* **2005**, *7*, 64−82.
(54) Levitt, M. H. *Spin Dynamics*; John Wiley and Sons Ltd.: England, 2008; Vol. 2.
(55) Dai, J.; Alaei, Z.; Plazzotta, B.; Pedersen, J. S.; Furó, I. Release of Solubilizate from Micelle upon Core Freezing. *J. Phys. Chem. B* **2017**, *121*, 10353−10363.
(56) Doncom, K. E. B.; Pitto-Barry, A.; Willcock, H.; Lu, A.; McKenzie, B. E.; Kirby, N.; O'Reilly, R. K. Complementary light scattering and synchrotron small-angle X-ray scattering studies of the micelle-to-unimer transition of polysulfobetaines. *Soft Matter* **2015**, *11*, 3666−3676.

https://doi.org/10.1021/acs.macromol.1c00635
Macromolecules 2021, 54, 6975−6981